VIP Hydrogen Evolution Very Important Paper

International Edition: DOI: 10.1002/anie.201510642
German Edition: DOI: 10.1002/ange.201510642

Oxyhydroxide Nanosheets with Highly Efficient Electron–Hole Pair Separation for Hydrogen Evolution

Junheng Huang[+], Qichao Shang[+], Yuanyuan Huang, Fumin Tang, Qun Zhang, Qinghua Liu, Shan Jiang, Fengchun Hu, Wei Liu, Yi Luo, Tao Yao,* Yong Jiang, Zhiyun Pan, Zhihu Sun, and Shiqiang Wei**

Abstract: *The facile electron–hole pair recombination in earth-abundant transition-metal oxides is a major limitation for the development of highly efficient hydrogen evolution photocatalysts. In this work, the thickness of a layered β-CoOOH semiconductor that contains metal/hydroxy groups was reduced to obtain an atomically thin, two-dimensional nanostructure. Analysis by ultrafast transient absorption spectroscopy revealed that electron–hole recombination is almost suppressed in the as-prepared 1.3 nm thick β-CoOOH nanosheet, which leads to prominent electron–hole separation efficiencies of 60–90 % upon irradiation at 350–450 nm, which are ten times higher than those of the bulk counterpart. X-ray absorption spectroscopy and first-principles calculations demonstrate that [HO−CoO_{6-x}] species on the nanosheet surface promote H^+ adsorption and H_2 desorption. An aqueous suspension of the β-CoOOH nanosheets exhibited a high hydrogen production rate of 160 μmol g^{-1} h^{-1} even when the system was operated for hundreds of hours.*

Since the photoreduction of water into hydrogen on TiO_2 was discovered in 1972,[1] the production of H_2 from water and alcohol solutions by semiconductor photocatalysis has become a fascinating scientific and technological means to store solar energy in clean chemical fuels.[2] Although TiO_2 can effectively photocatalyze H_2 evolution in water solutions, its wide band gap of 3.2 eV restricts the photoresponse to approximately 5 % of the UV region and thus seriously reduces the overall photoconversion efficiency.[3] Earth-abundant transition-metal oxides (TMOs) are attractive candidates for photocatalytic H_2 evolution materials, as they possess energy gaps ranging from 1 to 3 eV and can absorb visible light to generate electron–hole pairs.[4] In hydrogen evolution reactions (HERs) initiated by irradiation, a key step is the separation of the photoexcited electrons in the TMO material from the holes and their transfer to catalytically active surface sites for the reduction of H^+ to H_2. However, for most TMOs, the carrier diffusion length is short (ca. 2–4 nm for Fe_2O_3), and separation of the electron–hole pairs is inefficient because of the poor electrical conductivity of the materials.[5] Therefore, the development of TMO photocatalysts with efficient electron–hole separation is highly desirable for solar-to-chemical energy conversion, but also very challenging.

During the past two decades, great efforts have been devoted to modifying the electronic properties of TMOs by doping with various elements and the design of heterogeneous and nanoscale structures.[6] For instance, doping Ni into $InTaO_4$ can create new impurity energy levels within the band gap to prolong the lifetime of the photogenerated charge carriers, achieving a quantum efficiency of 0.66 % at 420 nm. However, these impurity dopants also serve as electron–hole recombination centers.[6a] Heterogeneous structures composed of two different semiconductor components (i.e., $Ga_{1-x}Zn_xN_{1-x}O_x$) were used to improve visible-light absorption, leading to a quantum efficiency of 2.5 % in 420–440 nm.[6b] Nonetheless, the interface between the two components incurred new kinetic problems for the transfer of the photogenerated charge carriers. Recently, a 10 nm nanocrystalline CoO photocatalyst with an enlarged surface area was reported to exhibit a remarkable quantum efficiency of 5 %.[6c] However, this catalyst became deactivated after only one hour, which was attributed to the poisoning of catalytic sites by the aggregation of holes at the nanoparticle surface. Therefore, developing a new strategy to efficiently separate electron–hole pairs in TMO materials is critical for achieving excellent photocatalytic HER activity. Recently, two-dimensional (2D) atomically thin nanosheets have shown remarkable advantages for improving photoelectrochemical performance.[7] As these 2D nanosheets are ultrathin, the carrier transfer distance is shortened, and the electronic structure is modified, which is beneficial for fast photoelectrochemical reactions. Therefore, the emergence of 2D ultrathin nanosheets gives us a hint that electron–hole recombination can be avoided by thinning the materials into atomically nanostructures.

Inspired by the ultrathin thickness, large surface area, and 2D confinement effects of nanosheets, we herein decreased the thickness of an oxyhydroxide semiconductor to obtain an atomically thin 2D nanosheet with efficient electron–hole pair separation, achieving 60–90 % electron–hole separation

[*] J. H. Huang,[+] Dr. Y. Y. Huang, F. M. Tang, Dr. Q. H. Liu, S. Jiang, F. C. Hu, W. Liu, Dr. T. Yao, Dr. Y. Jiang, Dr. Z. Y. Pan, Dr. Z. H. Sun, Prof. S. Q. Wei
National Synchrotron Radiation Laboratory
University of Science and Technology of China
Hefei 230029 (P. R. China)
E-mail: qhliu@ustc.edu.cn
yaot@ustc.edu.cn
sqwei@ustc.edu.cn
Q. C. Shang,[+] Prof. Q. Zhang, Prof. Y. Luo
Hefei National Laboratory for Physical Sciences at the Microscale
University of Science and Technology of China
Hefei 230026 (P. R. China)
[+] These authors contributed equally to this work.

Supporting information for this article is available on the WWW under http://dx.doi.org/10.1002/anie.201510642.

efficiencies at 350–450 nm. We choose β-CoOOH as our model substrate as it is structurally and catalytically stable compared with CdS, and displays a relatively narrow band gap for visible-light absorption compared with TiO_2. Moreover, in layered β-CoOOH, the octahedral metal/hydroxy structure at the layer surface (see Figure 1 a) is beneficial for proton reduction and H_2 desorption.[8a] Furthermore, the exposure of

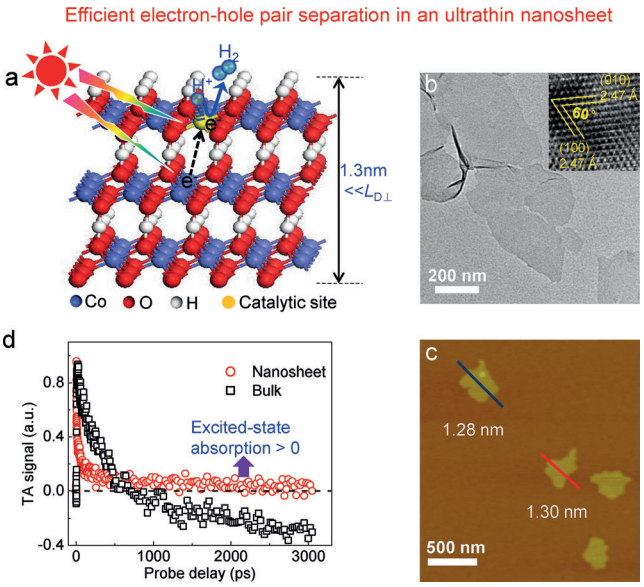

Figure 1. a) Schematic representation of the effects in two-dimensional β-CoOOH nanosheets. $L_{D\perp}$ denotes the carrier diffusion length along the *c* axis. b) TEM, HRTEM (inset), and c) AFM images of the β-CoOOH nanosheets. d) Ultrafast transient absorption signal (probed at 520 nm) as a function of probe delay for β-CoOOH nanosheets with bulk β-CoOOH as the reference, recorded with a 400 nm pump.

hydroxy groups on the nanosheet surface would render the hydrogen evolution reaction thermodynamically more neutral.[8] The thickness (1.3 nm) of the nanosheet is much smaller than the carrier diffusion length along the *c* axis, and photocarriers can thus be directly transferred to catalytically active surface sites, overcoming the notorious photocarrier recombination pathways encountered in the bulk counterpart (Figure 1 a). Meanwhile, in the ultrathin nanosheet, the surface area, with abundant, active CoO_{6-x} centers that can immediately capture the photocarriers to participate in the photocatalytic reaction, accounts for a large proportion (>67%) of the overall material. Furthermore, the 2D confinement effect in the β-CoOOH nanosheet induces a negative shift of the conduction band, which could also improve the photocatalytic hydrogen evolution capability. Consequently, the obtained β-CoOOH nanosheet suspension can effectively photocatalyze H_2 evolution from aqueous alcohol solutions with quantum efficiencies of 1–3% when irradiated at 350–450 nm. Moreover, the β-CoOOH nanosheet maintained a high rate of hydrogen production with robust stability when reused 60 times.

The β-CoOOH nanosheets were obtained by a two-step phase transformation strategy (for details see the Supporting Information). The formation of atomically thin β-CoOOH nanosheets was confirmed by transmission electron microscopy (TEM; Figure 1 b) and atomic force microscopy (AFM; Figure 1 c). Statistical height profiles revealed the thickness of the nanosheet to be about 1.3 nm (Figure 1 c; see also the Supporting Information, Figure S2). The high-resolution TEM (HRTEM) image of the β-CoOOH nanosheets shows distinct lattice fringes of 0.247 nm with 60° angles, which were attributed to the (010) and (100) planes of β-CoOOH, suggesting the exposure of the (001) facets of the β-CoOOH matrix. The X-ray diffraction (XRD) patterns also support the hypothesis that the (001) facets of the nanosheet are exposed (Figure S3). These results provide solid evidence that atomically thin β-CoOOH nanosheets have been successfully fabricated.

To gain insight into the electronic properties of the β-CoOOH nanosheets, they were analyzed by ultrafast transient absorption (TA) spectroscopy (for details see the Supporting Information), a robust method to track, in real time, the dynamics of photoexcited carriers in nanomaterials.[9] As shown in Figure 1 d, the positive TA signal can be ascribed to excited-state absorption (ESA), whereas the negative one was attributed to stimulated emission (SE).[10] For the β-CoOOH nanosheet, the TA signals are dominated by the positive ESA transients over the whole time range. In contrast, around 600 ps after photoexcitation, the bulk counterpart exhibited a negative SE transient that arises from the radiative recombination of energized electrons with holes.[11] The complete disappearance of SE transients for the nanosheet strongly suggests that electron–hole recombination has been significantly suppressed, and that the photocarriers in the ground state have been substantially depleted throughout the nanosheet surface.

Furthermore, the charge separation (CS) efficiency of the nanosheet is as high as almost 90% under UV irradiation and greater than 60% under visible-light irradiation (400–450 nm; Figure 2 a, for details see the Supporting Information). In contrast, the CS efficiency of the bulk material is less than 10% independent of the wavelength of the incident light, and thus one order of magnitude lower than that of the nanosheet. The CS efficiency measurements further consolidate the fundamental role of the atomic thickness in separating the photocarriers in the nanosheet. Moreover, electrochemical impedance spectra show that the radius of the semicircular Nyquist plot for the β-CoOOH nanosheet (130 Ω) is much smaller than that of the bulk counterpart (200 Ω), indicating a low charge-transfer resistance in the nanosheet (Figure 2 b). These results, together with the TA spectroscopic characterization, demonstrate efficient electron–hole pair separation in the β-CoOOH nanosheet, which is beneficial for obtaining an improved photocatalyst.

To examine the solar H_2 evolution activity, we determined the H_2 production and quantum efficiency (QE) from an aqueous methanol solution catalyzed by the as-prepared β-CoOOH nanosheets under standard reaction conditions and with a standard measurement apparatus.[6a] The typical time course of H_2 evolution over the β-CoOOH nanosheets is shown in Figure 2 c. The constant H_2 evolution rate was evaluated as 160 $\mu mol\,h^{-1}\,g^{-1}$ for the β-CoOOH nanosheet photocatalyst, whereas comparative tests showed that nearly

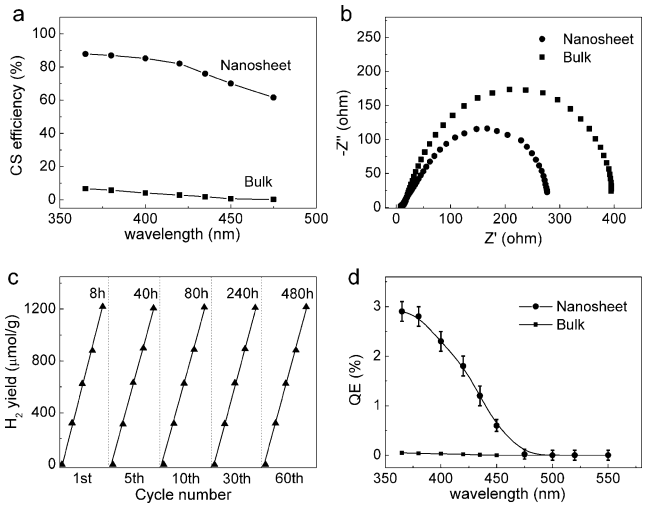

Figure 2. a) Charge separation (CS) efficiencies of the β-CoOOH nanosheets and the bulk material as a function of the wavelength of the incident light. b) Electrochemical impedance spectra for nanosheet and bulk β-CoOOH. c) Typical time course of the hydrogen production from an aqueous methanol solution under simulated sunlight irradiation. d) QE curve of a β-CoOOH nanosheet suspension and the bulk material in aqueous alcohol solution.

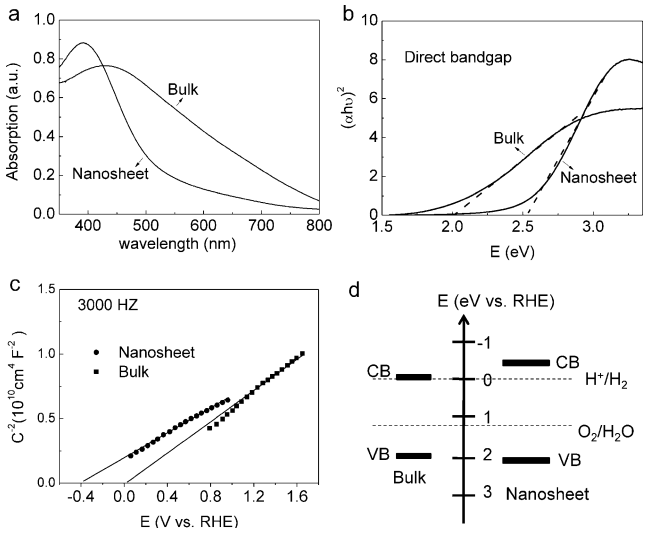

Figure 3. a) UV/Vis absorption spectra of bulk and nanosheet β-CoOOH. b) Absorption spectra of β-CoOOH nanosheets and bulk β-CoOOH plotted as $(h\nu\alpha)^n$ as a function of the photon energy. c) Mott–Schottky plots of β-CoOOH nanosheets and bulk β-CoOOH measured in the dark. d) The band structure of bulk and nanosheet β-CoOOH.

no H_2 evolution was observed when bulk β-CoOOH was used as the photocatalyst. The total number of electrons participating in the H_2 evolution process over 480 hours amounted to 1.5 mmol, far exceeding the amount (0.1 mmol) of photocatalyst used in the reaction. The quantum efficiency of H_2 evolution over the β-CoOOH nanosheet photocatalyst as a function of the wavelength of the incident light is shown in Figure 2d. It is worth noting that the quantum efficiency of the β-CoOOH nanosheets is close to 3% in the UV region and over 2% at 420 nm. In contrast, the quantum efficiency of bulk β-CoOOH is quite low in both the UV and visible-light region, which is due to the low energy of its conduction band edge (Figure 3d) and the small proportion of surface atoms. Furthermore, the β-CoOOH nanosheet maintained a high rate of H_2 production (ca. 160 $\mu mol\,h^{-1}g^{-1}$) with robust stability when recycled 60 times.

To disclose variations in the optical properties and the band alignment of the β-CoOOH nanosheets, they were analyzed by UV/Vis absorption spectroscopy and the Mott–Schottky method (Figure 3a–c). The absorption edge of the β-CoOOH nanosheets is blue-shifted with respect to the bulk material (Figure 3a). The fitting results, which were obtained by using the Tauc/Davis–Mott expression, $(h\nu\alpha)^{1/n} = A(h\nu - E_g)$, indicated that the band gap of material was enlarged from 2.0 eV for the bulk material to 2.5 eV in the nanosheet (Figure 3b). The flat-band potential extrapolated for the β-CoOOH nanosheets is about −0.3 V versus the reversible hydrogen electrode (RHE), which is significantly more negative than that of the bulk compound (ca. 0 V). For n-type semiconductors, the flat-band potential is 0–0.1 V higher than the conduction-band potential.[4c] This means that the conduction-band minimum (CBM) in the β-CoOOH nanosheets is negatively shifted by about 0.4 eV, and now surpasses the hydrogen evolution potential (Figure 3d), thus satisfying the thermodynamic requirements for hydrogen evolution under solar irradiation.

The atomic structures of the samples were investigated by X-ray absorption fine structure spectroscopy (XAFS). From the Co K-edge $k^3\chi(k)$ oscillation curve (Figure 4a), an obvious oscillation damping at 2–8 $Å^{-1}$ was observed for the nanosheet. Moreover, the Fourier transform (FT) curves of the nanosheet in Figure 4b show that the intensities of the FT peaks at 1.48 Å and 2.50 Å were noticeably reduced. These results imply that the Co atoms are not fully coordinated, which was confirmed by the reduced Co–O coordination number (5.0) that was obtained by quantitative extended XAFS fitting (Table S1). This finding indicates the distortion of the surface structure and the presence of unsaturated

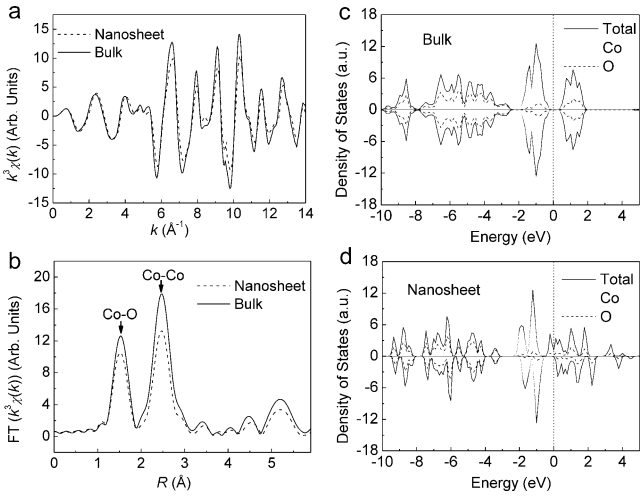

Figure 4. a) Co K-edge EXAFS $k^3\chi(k)$ oscillation functions and b) the corresponding FT curves of bulk and nanosheet β-CoOOH. Calculated density of states for bulk (c) and nanosheet (d) β-CoOOH.

Co–O coordination (CoO_{6-x}) at the surface. Based on the structural model derived from the XAFS results, we performed first-principles band-structure calculations. Whereas the antibonding e_g orbitals are empty in bulk β-CoOOH, about 30% of the e_g orbitals are occupied in the nanosheet (Figure 4c,d), which might be due the incorporation of CoO_{6-x} motifs and 2D confinement effects. In particular, the octahedral cobalt–hydroxy motifs (HO-CoO_{6-x} octahedra) are arranged perpendicularly to the (010) plane along the *a* axis (Figure 1a). Owing to the geometry of the HO–CoO_{6-x} octahedron, the antibonding e_g orbitals of the surface Co ions overlap directly with those of adsorbed species (Figure 4d). Hence, the partially occupied e_g orbitals in β-CoOOH nanosheets can promote electron transfer between surface cations and H^+.[12] On the other hand, considering the thermochemistry of the hydrogen evolution reaction, the activity of a catalytic site can be judged by the adsorption free energy of H* (ΔG(H*)), where H* denotes a hydrogen atom adsorbed on the catalytic surface.[13a] Compared to pure CoO_{6-x}, the Co sites in the hydroxy-dominated HO-CoO_{6-x} surface of CoOOH nanosheets would have a smaller absolute ΔG(H*) value, which could effectively equilibrate the thermodynamics of H^+ adsorption and H_2 desorption on the catalytic sites.[13b] As a result, the cleavage of [Co(OH)–H] to release H_2 is significantly facilitated. Furthermore, owing to the ultrathin nature (1.3 nm thick) of the nanosheet (smaller than $L_{D\perp}$), the photocarriers can be easily and quickly transferred to the surface (Figure 1a), similar to in a nanoporous $BiVO_4$ photocatalyst.[14] Consequently, the photocarriers captured by the surface CoO_{6-x} catalytic sites could be efficiently used to reduce the protons, accelerating electron transfer and increasing the HER activity.

In summary, by downsizing an oxyhydroxide β-CoOOH semiconductor to obtain atomically thin nanosheets, poorly efficient photocarrier transportation and electron–hole pair recombination, which are often encountered in TMO semiconductors, have been successfully overcome. Ultrafast TA spectroscopy clearly revealed that electron–hole recombination in the as-prepared 1.3 nm thick β-CoOOH nanosheet is almost suppressed, which leads to prominent charge separation efficiencies of 60–90% in 350–450 nm. A β-CoOOH nanosheet suspension exhibited a high hydrogen production rate of 160 $\mu mol\,g^{-1}\,h^{-1}$, even when operated for hundreds of hours. The insights gained from XAFS and first-principles calculations provide strong evidence for the hypothesis that a rearrangement of the surface structure leads to the formation of HO–CoO_{6-x} species on the nanosheet surface, which can effectively equilibrate the thermodynamics of H^+ adsorption and H_2 desorption on the catalytic sites, thus greatly accelerating electron transfer and improving the HER activity. These results highlight that a stable and economic hydrogen evolution photocatalyst based on a transition-metal oxyhydroxide has been developed for the production of clean energy.

Acknowledgements

This work was supported by the National Basic Research Program of China (2012CB825800 and 2010CB923300), the National Natural Science Foundation of China (21533007, 11135008, U1332111, U1532265, 11435012, 11305174, 11422547, 21173205, 21573211, 21471143, 11305172, and 91127042), the Foundation for Innovative Research Groups of the National Natural Science Foundation of China (11321503), the Chinese Academy of Sciences (XDB01020000), and the Fundamental Research Funds for the Central Universities (WK2340000063, WK2310000050, and KY2310000019). We would like to thank NSRL, BSRF, and SSRF for synchrotron beam time.

Keywords: cobalt · hydrogen evolution · nanosheets · XAFS spectroscopy

How to cite: *Angew. Chem. Int. Ed.* **2016**, *55*, 2137–2141
Angew. Chem. **2016**, *128*, 2177–2181

[1] A. Fujishima, K. Honda, *Nature* **1972**, *238*, 37.
[2] a) M. G. Walter, E. L. Warren, J. R. McKone, S. W. Boettcher, Q. X. Mi, E. A. Santori, N. S. Lewis, *Chem. Rev.* **2010**, *110*, 6446–6473; b) J. Liu, Y. Liu, N. Liu, Y. Han, X. Zhang, H. Huang, Y. Lifshitz, S.-T. Lee, J. Zhong, Z. Kang, *Science* **2015**, *347*, 970–974; c) H. Zhiji, Q. Fen, R. Eisenberg, P. L. Holland, T. D. Krauss, *Science* **2012**, *338*, 1321–1324.
[3] a) R. Asahi, T. Morikawa, T. Ohwaki, K. Aoki, Y. Taga, *Science* **2001**, *293*, 269–271; b) X. B. Chen, L. Liu, P. Y. Yu, S. S. Mao, *Science* **2011**, *331*, 746–750.
[4] a) L. M. Peter, K. G. U. Wijayantha, *ChemPhysChem* **2014**, *15*, 1983–1995; b) X. B. Chen, S. H. Shen, L. J. Guo, S. S. Mao, *Chem. Rev.* **2010**, *110*, 6503–6570; c) M. Grätzel, *Nature* **2001**, *414*, 338–344.
[5] a) Q. H. Liu, J. F. He, T. Yao, Z. H. Sun, W. R. Cheng, S. He, Y. Xie, Y. H. Peng, H. Cheng, Y. F. Sun, Y. Jiang, F. C. Hu, Z. Xie, W. S. Yan, Z. Y. Pan, Z. Y. Wu, S. Q. Wei, *Nat. Commun.* **2014**, *5*, 5122; b) R. D. L. Smith, M. S. Prevot, R. D. Fagan, Z. P. Zhang, P. A. Sedach, M. K. J. Siu, S. Trudel, C. P. Berlinguette, *Science* **2013**, *340*, 60–63.
[6] a) Z. G. Zou, J. H. Ye, K. Sayama, H. Arakawa, *Nature* **2001**, *414*, 625–627; b) K. Maeda, K. Teramura, D. L. Lu, T. Takata, N. Saito, Y. Inoue, K. Domen, *Nature* **2006**, *440*, 295; c) L. B. Liao, Q. H. Zhang, Z. H. Su, Z. Z. Zhao, Y. N. Wang, Y. Li, X. X. Lu, D. G. Wei, G. Y. Feng, Q. K. Yu, X. J. Cai, J. M. Zhao, Z. F. Ren, H. Fang, F. Robles-Hernandez, S. Baldelli, J. M. Bao, *Nat. Nanotechnol.* **2014**, *9*, 69–73; d) X. B. Chen, C. Burda, *J. Am. Chem. Soc.* **2008**, *130*, 5018–5019; e) P. Wang, J. Zhang, H. L. He, X. L. Xu, Y. D. Jin, *Nanoscale* **2015**, *7*, 5767–5775; f) S. U. M. Khan, M. Al-Shahry, W. B. Ingler, *Science* **2002**, *297*, 2243–2245.
[7] a) C. L. Tan, H. Zhang, *Nat. Commun.* **2015**, *6*, 7873; b) A. K. Geim, *Science* **2009**, *324*, 1530–1534; c) F. Schwierz, *Nat. Nanotechnol.* **2010**, *5*, 487–496; d) C. L. Tan, H. Zhang, *Chem. Soc. Rev.* **2015**, *44*, 2713–2731; e) X. Huang, Z. Y. Zeng, H. Zhang, *Chem. Soc. Rev.* **2013**, *42*, 1934–1946; f) H. Zhang, *ACS Nano* **2015**, *8*, 9451–9469; g) Z. Y. Yin, B. Chen, M. Bosman, X. H. Cao, J. Z. Chen, B. Zheng, H. Zhang, *Small* **2014**, *10*, 3537–3543.
[8] a) D. K. Bediako, B. Lassalle-Kaiser, Y. Surendranath, J. Yano, V. K. Yachandra, D. G. Nocera, *J. Am. Chem. Soc.* **2012**, *134*, 6801–6809; b) Y. Surendranath, M. W. Kanan, D. G. Nocera, *J. Am. Chem. Soc.* **2010**, *132*, 16501–16509.

[9] a) Q. Zhang, H. J. Zheng, Z. G. Geng, S. L. Jiang, J. Ge, K. L. Fan, S. Duan, Y. Chen, X. P. Wang, Y. Luo, *J. Am. Chem. Soc.* **2013**, *135*, 12468 – 12474; b) L. L. Wang, J. Ge, A. L. Wang, M. S. Deng, X. J. Wang, S. Bai, R. Li, J. Jiang, Q. Zhang, Y. Luo, Y. J. Xiong, *Angew. Chem. Int. Ed.* **2014**, *53*, 5107 – 5111; *Angew. Chem.* **2014**, *126*, 5207 – 5211; c) B. Wu, J. H. Hu, P. Cui, L. Jiang, Z. W. Chen, Q. Zhang, C. R. Wang, Y. Luo, *J. Am. Chem. Soc.* **2015**, *137*, 8769 – 8774; d) F. C. Lei, L. Zhang, Y. F. Sun, L. Liang, K. T. Liu, J. Q. Xu, Q. Zhang, B. C. Pan, Y. Luo, Y. Xie, *Angew. Chem. Int. Ed.* **2015**, *54*, 9266 – 9270; *Angew. Chem.* **2015**, *127*, 9398 – 9402.

[10] S. Bai, J. Jiang, Q. Zhang, Y. J. Xiong, *Chem. Soc. Rev.* **2015**, *44*, 2893 – 2939.

[11] S. Bai, J. Ge, L. L. Wang, M. Gong, M. S. Deng, Q. Kong, L. Song, J. Jiang, Q. Zhang, Y. Luo, Y. Xie, Y. J. Xiong, *Adv. Mater.* **2014**, *26*, 5689 – 5695.

[12] J. Suntivich, K. J. May, H. A. Gasteiger, J. B. Goodenough, Y. Shao-Horn, *Science* **2011**, *334*, 1383 – 1385.

[13] a) J. K. Nørskov, T. Bligaard, A. Logadottir, J. R. Kitchin, J. G. Chen, S. Pandelov, U. Stimming, *J. Electrochem. Soc.* **2005**, *152*, J23 – J26; b) M. Zhang, M. de Respinis, H. Frei, *Nat. Chem.* **2014**, *6*, 362 – 367.

[14] T. W. Kim, K. S. Choi, *Science* **2014**, *343*, 990 – 994.

Received: November 17, 2015
Published online: January 6, 2016

